



Communication

# Co-Catalyzed Asymmetric Hydrogenation. The Same Enantioselection Pattern for Different Mechanisms

Ilya D. Gridnev 

N. D. Zelinsky Institute of Organic Chemistry, Russian Academy of Sciences, Leninsky Prospekt 47, 119911 Moscow, Russia; ilyaiochem@gmail.com

**Abstract:** The mechanism of the recently reported catalyzed asymmetric hydrogenation of enyne **1** catalyzed by the Co-(*R,R*)-QuinoxP\* complex was studied by DFT. Conceivable pathways for the Co(I)-Co(III) mechanism were computed together with a Co(0)-Co(II) catalytic cycle. It is commonly assumed that the exact nature of the chemical transformations taking place along the actually operating catalytic pathway determine the sense and level of enantioselection of the catalytic reaction. In this work, two chemically different mechanisms reproduced the experimentally observed perfect stereoselection of the same handedness. Moreover, the relative stabilities of the transition states of the stereo induction stages were controlled via exactly the same weak disperse interactions between the catalyst and the substrate.

**Keywords:** asymmetric catalysis; asymmetric hydrogenation; DFT computation; mechanism of stereoselection; weak intramolecular interactions

## 1. Introduction

Obtaining a better understanding of the intrinsic mechanisms for generating chirality via asymmetric catalysis is one of the most important current targets of chemical research [1,2]. Although significant progress has been made in the experimental characterization of reactive intermediates, as well as in computational studies of various catalytic cycles, the results accumulated to date lack sufficient generalization and classification, with each particular reaction being considered as a specific case with its own mechanism of chirality generation. Even the simplest conceivable asymmetric catalytic reaction, viz., asymmetric hydrogenation, is a field comprising a lot of different suggestions, mechanistic ideas, reconsiderations, empirical rules, etc. [3–23].

This situation has become still more complicated with the recent rapid development of new hydrogenation techniques applying asymmetric catalysis with complexes of cheap and abundant metals [24–26]. Numerous mechanistic studies of the catalytic cycles of asymmetric hydrogenations have been performed of catalysis by earth-abundant metals, such as Ni [27–31], Co [32–47], Fe [48–52], Mn [53,54], etc. It seems that each metal has its own hydrogenation chemistry, which can in turn be subdivided into various catalytic cycles with different metal oxidation states.

Recently, Zhang et al. reported co-catalyzed asymmetric hydrogenation of enynes and suggested Co(I)-Co(III), with a mechanism based on analogous Rh-catalyzed reactions being suggested (Scheme 1) [46]. Being interested in the mechanisms of stereoselection in various catalytic asymmetric reactions, the author decided to study the mechanism of this new reaction computationally. Unexpectedly it was found that different mechanisms, either Co(I)-Co(III) or Co(0)-Co(II), which are dissimilar in their chemical details and the structures of their intermediates, predict the same sense and level of enantioselectivity.



**Citation:** Gridnev, I.D. Co-Catalyzed Asymmetric Hydrogenation. The Same Enantioselection Pattern for Different Mechanisms. *Int. J. Mol. Sci.* **2023**, *24*, 5568. <https://doi.org/10.3390/ijms24065568>

Academic Editor: Maxim V. Musalov

Received: 18 February 2023

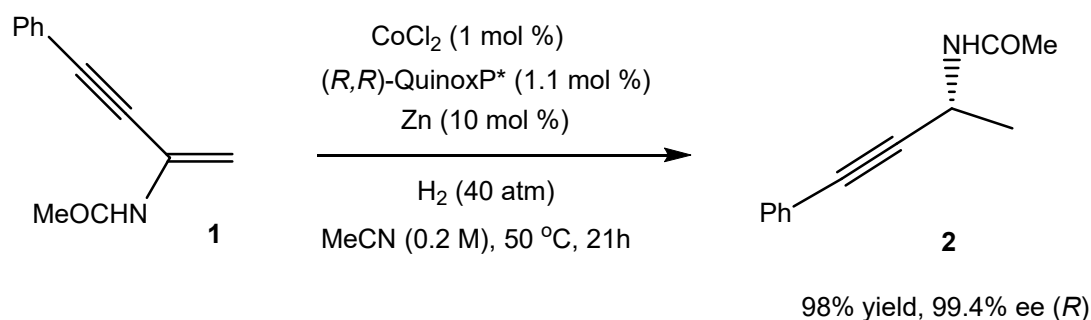
Revised: 3 March 2023

Accepted: 7 March 2023

Published: 14 March 2023



**Copyright:** © 2023 by the author. Licensee MDPI, Basel, Switzerland. This article is an open access article distributed under the terms and conditions of the Creative Commons Attribution (CC BY) license (<https://creativecommons.org/licenses/by/4.0/>).



**Scheme 1.** Asymmetric hydrogenation of 1.

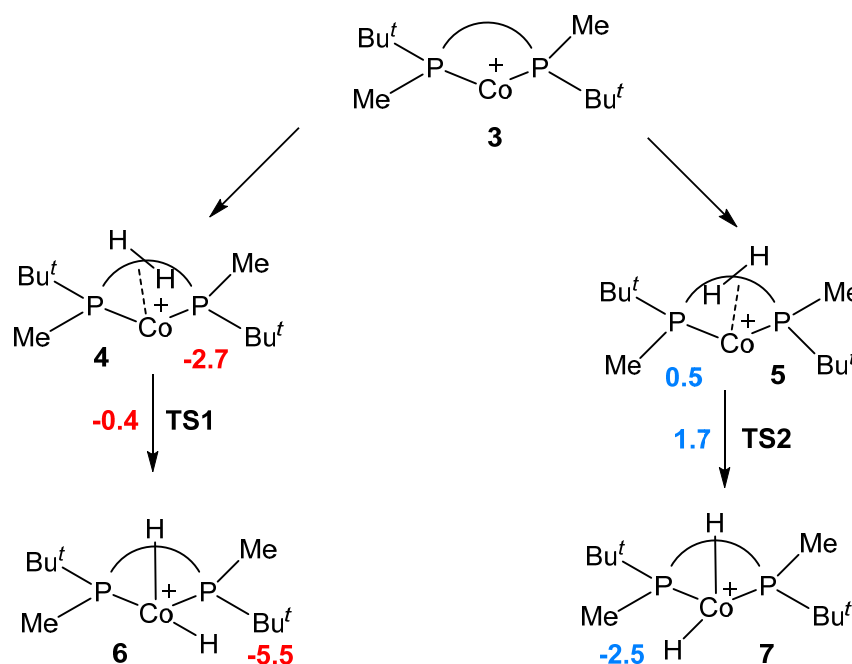
The author is convinced that this is an important finding for a general theory of asymmetric catalysis, and presents the results in this paper.

## 2. Results and Discussion

The authors suggest a Co(I)-Co(III) mechanism for the reaction based on the analogous synthesis of the corresponding Rh-catalyzed hydrogenation [46]. Hence, the corresponding competing catalytic cycles were first computed.

### 2.1. Formation of Solvate Dihydrides

QuinoxP\*-Co(I) complex 3 was computed to undergo facile hydrogenation yielding diastereomeric solvate dihydrides 6 and 7 via initial formation of molecular hydrogen complexes 4 and 5 (Scheme 2).

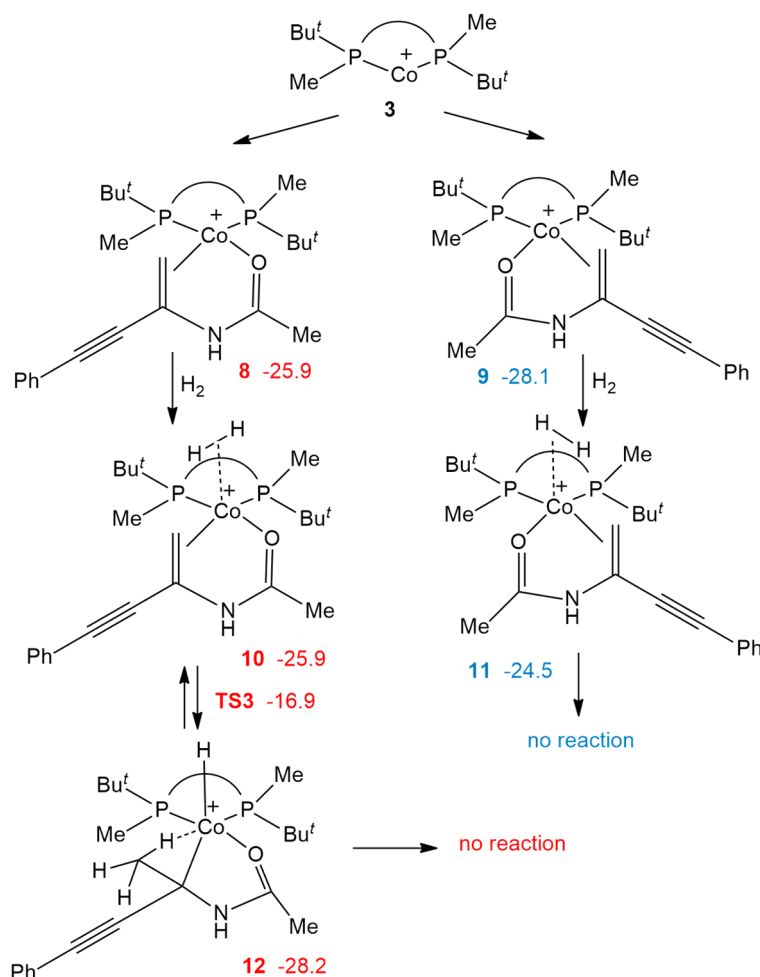


**Scheme 2.** Formation of dihydride complexes 6 and 7. The solvent molecules were not computed explicitly, and are not shown in this schematic representation. Computed free energies are given relative to  $3 + 1 + \text{H}_2$  (shown in red and blue for opposite enantiomers).

It was concluded that these hydrogenations are suitable reactions for the dihydrogen activation and can make a start for a Co(I)-Co(III) catalytic cycle.

## 2.2. Oxidative Addition to Catalyst–Substrate Complexes

Stable catalyst–substrate complexes **8** and **9** are formed upon the reaction of **3** with the substrate **1** (Scheme 3). They give corresponding molecular hydrogen complexes **10** and **11** upon reaction with dihydrogen. However, oxidative addition of  $H_2$  takes place only in complex **10**, whereas when a hydrogen atom approaches Co in complex **11**, a steady increase in energy results, and this does not lead to any productive transformation.



**Scheme 3.** Reaction of the catalyst–substrate complexes **8** and **9** with dihydrogen. Computed free energies are given relative to **3** + **1** +  $H_2$  (shown in red and blue for R- and S-pathways, respectively).

This could be a basis for a perfectly enantioselective reaction; however, the complex **12** is not capable of undergoing reductive elimination for the completion of the catalytic cycle. An extensive search for possible pathways of the reductive elimination in **12** invariably led to a reverse reaction, an exchange between two hydrides or dissociation of the double bond.

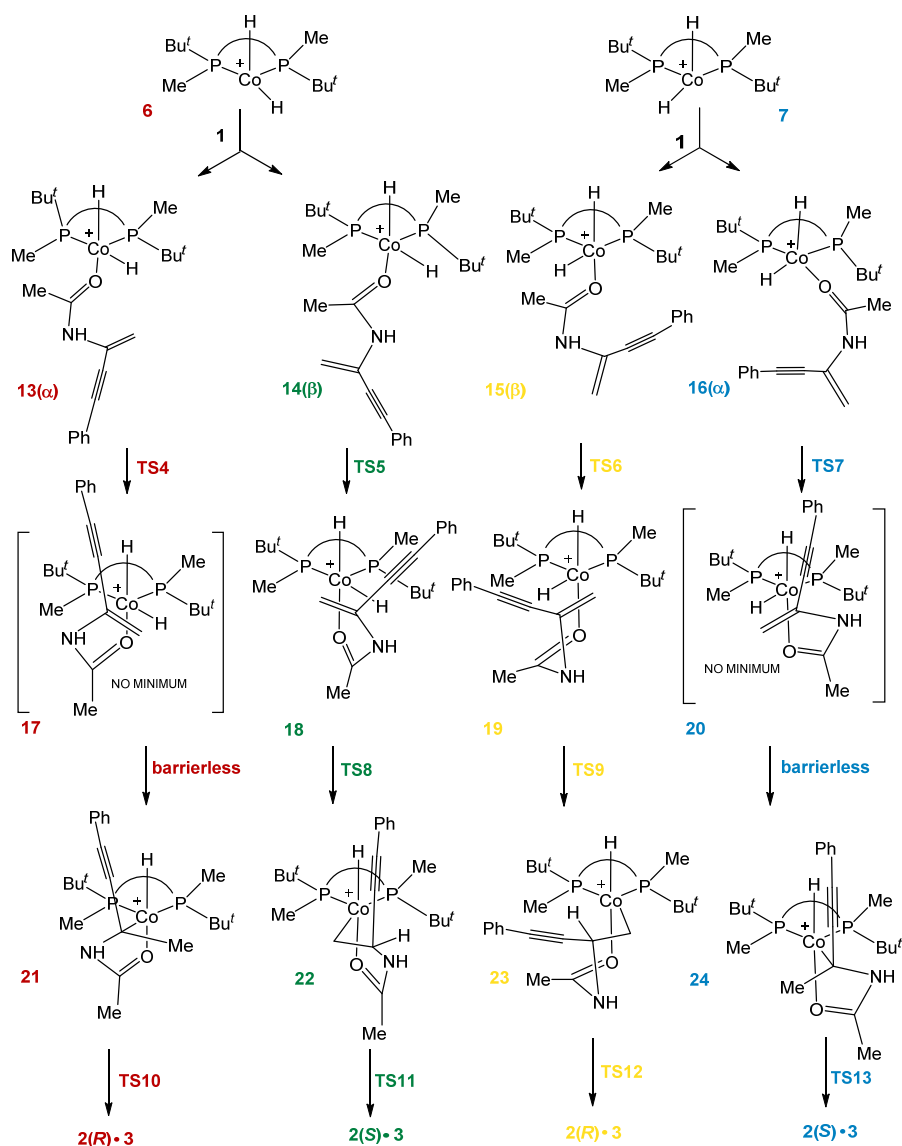
The same situation has previously been described for Rh-catalyzed asymmetric hydrogenations, where it was shown that dissociation of the double bond with its further re-association in the octahedral complexes is the most feasible pathway for reaction products [11,12].

Thus, the reaction of catalyst–substrate complexes with dihydrogen is unlikely to contribute to the flux of catalysis in the reaction under study.

## 2.3. Stereoselective Formation of Chelating Dihydrides—Four Competing Catalytic Cycles

As can be seen from the Scheme 3, the dihydride complexes **6** and **7** are stable and readily available intermediates. Therefore, their reactions with substrate **1** were studied (Scheme 4). Initially, encounter complexes **13**–**16** are formed. In these intermediates, the substrate is bound to the catalyst via coordination of the oxygen atom of the acetamido group

to Co and through the non-covalent interactions of the phenylpropynyl group with the *t*-Bu and Me substituents of the ligand. Further approach of the double bond to the Co-H unit can proceed, producing  $\alpha$ - or  $\beta$ - dihydride intermediates in each case, but only the  $\beta$ -dihydrides **18** and **19** could be located as definite minima. On the other hand, when the double bond in **13** and **16** achieved a proper orientation for the hydride transfer (coplanar to the Co-H bond *trans*- to phosphorus), immediate barrierless migratory insertion takes place yielding the corresponding monohydride intermediates **21** and **24**. Finally, the reductive elimination yields the product and recovers the catalyst in each of the four pathways (Scheme 4).



**Scheme 4.** Four competing pathways in the Co(I)-Co(III) mechanism of the asymmetric hydrogenation of **1** with Co complex **3**.

Scanning the approach of the double bond to the reactive site (Figure 1) revealed further details of the process of stereoselection during the formation of chelate cycles. Apparently, the discrimination between the  $\alpha$ - and  $\beta$ -pathways takes place at the early stage of this process. Thus, in the range of the interatomic differences 6–8 Å, the interconversion between the different pathways is facile through the rotations around ordinary bonds, and the Boltzmann distribution strongly favors the  $\alpha$ -pathways. Since at shorter interatomic distances the direct convergence between different pathways becomes impossible, the  $\beta$ -pathways can be excluded from the consideration.

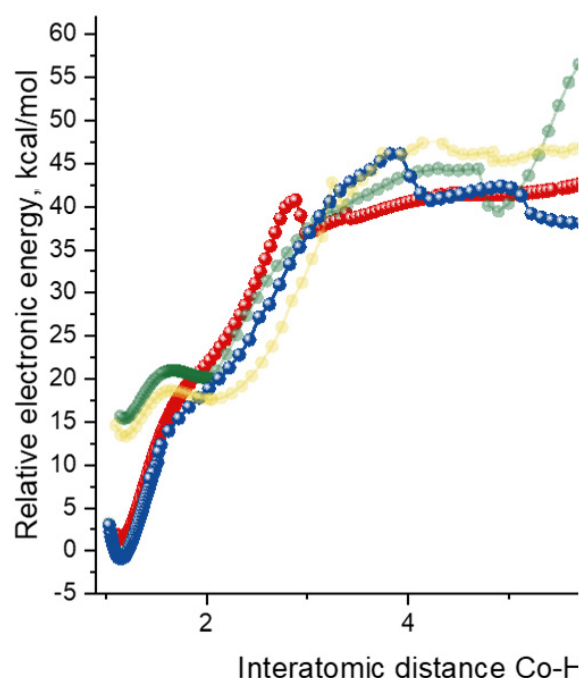


**Figure 1.** Scans of the electronic energy changes upon approach of the double bond towards the appropriate configuration for the migratory insertion step. Red— $R(\alpha)$ , blue— $S(\alpha)$ , yellow— $R(\beta)$ , green— $S(\beta)$ .

Both  $\alpha$ -pathways exhibit definite maxima at around 3 Å ( $R(\alpha)$  pathway) and around 4 Å ( $S(\alpha)$  pathway), due to the necessity of changing the pattern of the disperse interactions between the substrate and the catalyst. The difference between the free energies of the corresponding transition states **TS4** and **TS7** apparently determines the optical yield of the whole catalytic cycle (Figure 2), since there are no other maxima on the way towards the corresponding monohydride intermediates **21** and **24** and the barrier of the reductive elimination of the  $S(\alpha)$  pathway is significantly higher than that of the  $R(\alpha)$  pathway.

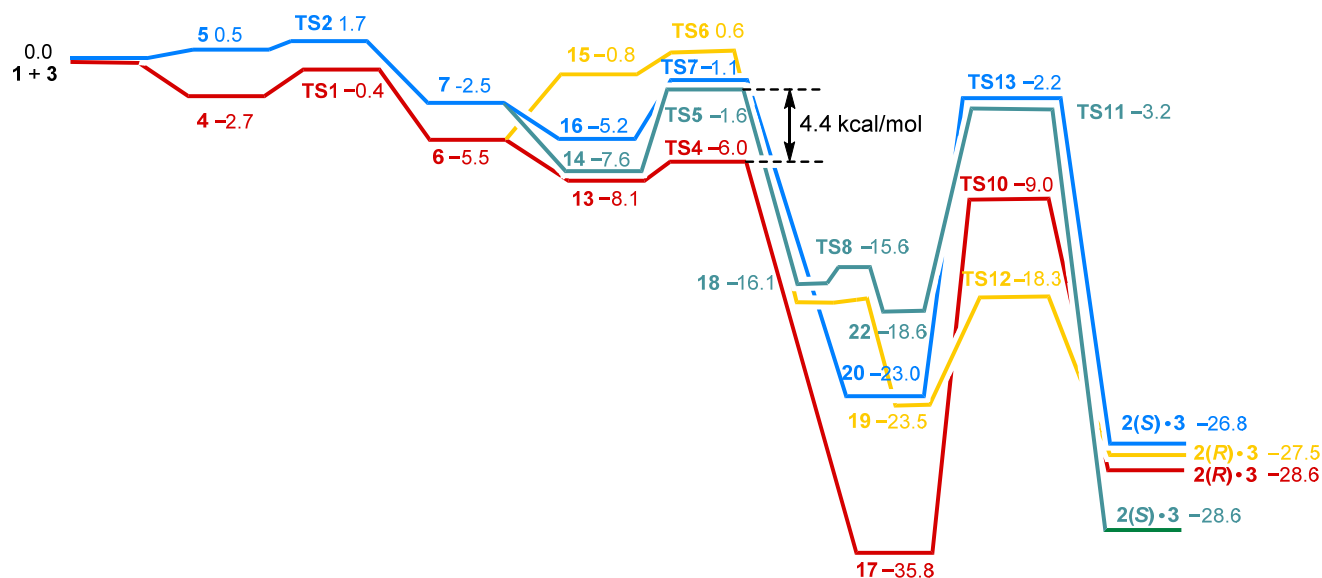


**Figure 2.** Profile of relative free energies (kcal/mol) in four competing catalytic cycles of the Co(I)-Co(III) route. Red— $R(\alpha)$ , blue— $S(\alpha)$ , yellow— $R(\beta)$ , green— $S(\beta)$ .

The optimized structures of **TS4** and **TS7** are shown in Figure 3. Comparing them, it can be concluded that the main contribution to the greater stability of the former originates from much more pronounced C-H  $\cdots \pi$  interactions of the acetylenic unit with the *t*-Bu group in the **TS4** compared to the same interactions of the Me group in the **TS7**, since all other stabilizing intramolecular interactions appear to be very similar in both structures. These observations promote the triple bond as an effective stereoregulating group.

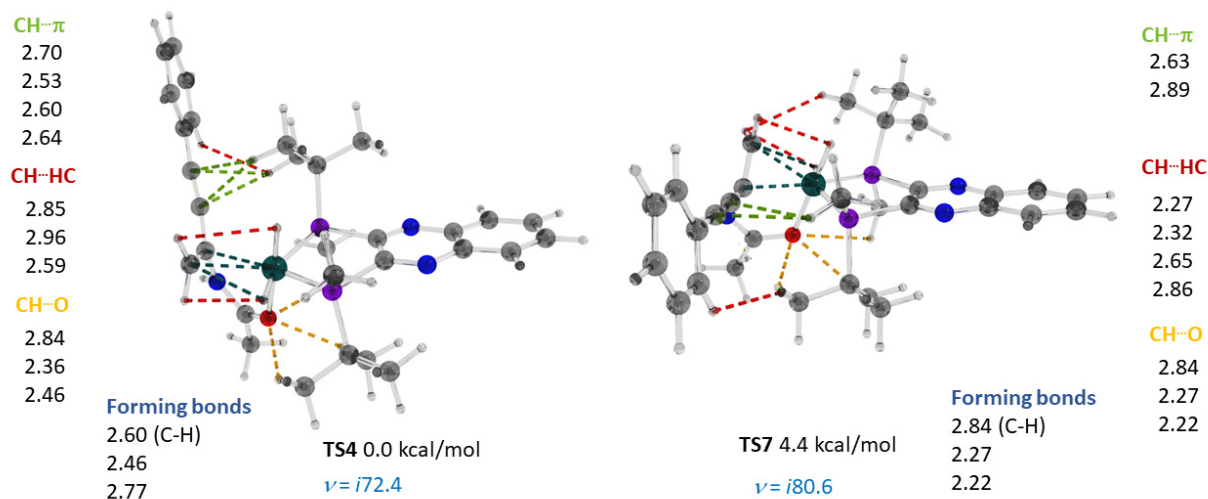


**Figure 3.** Optimized structures and important interatomic distances of the transition states **TS4** and **TS7**. Black—C, grey—H, blue—N, red—O, violet—P, turquoise—Co.

#### 2.4. Co(0)-Co(II) Mechanism

The reaction conditions applied in the experimental study suggest that a Co(0)-Co(II) mechanism is also conceivable. This consideration prompted computations of the corresponding catalytic cycles.

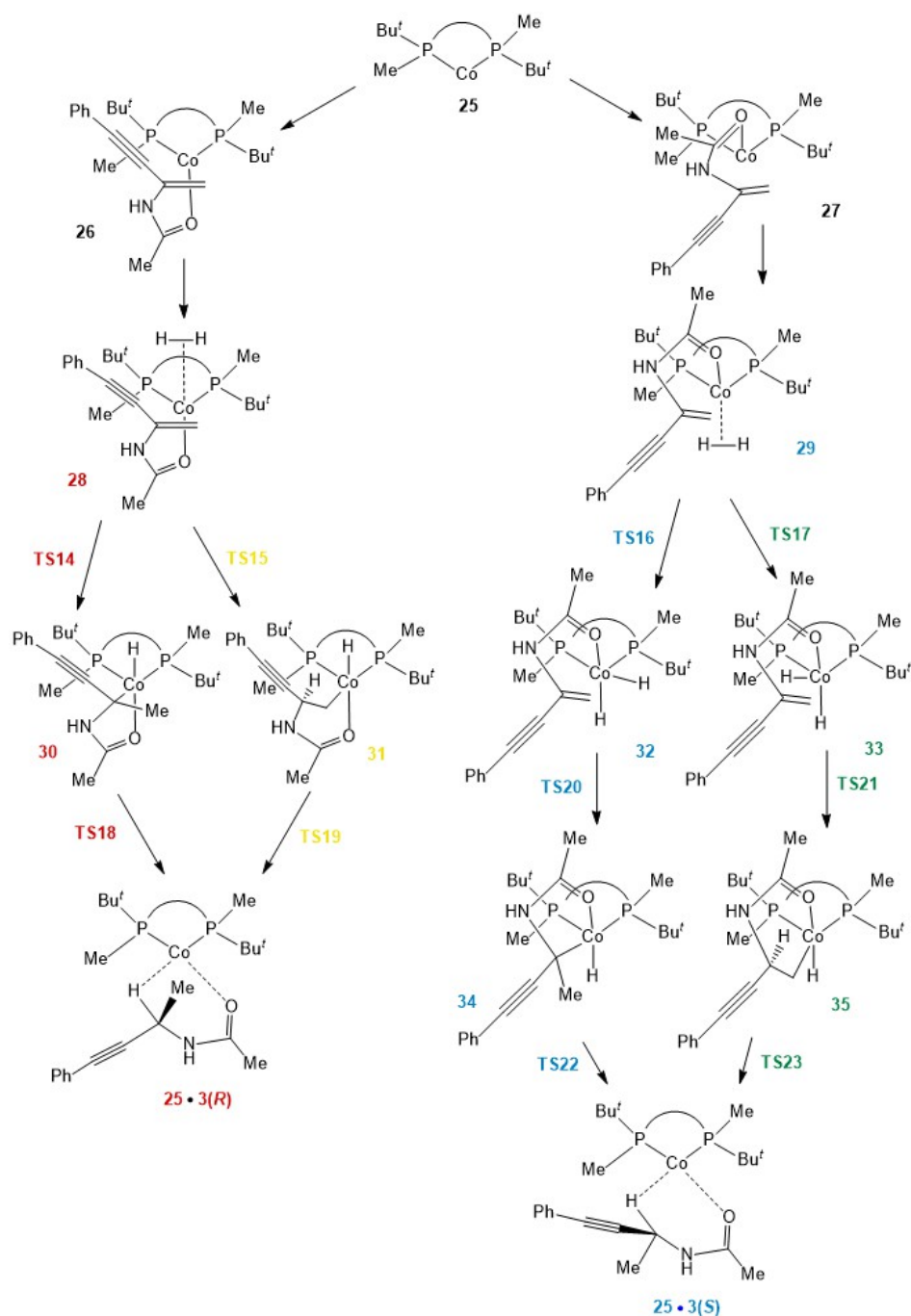
The substrate can coordinate to the neutral solvate complex of Co(0) **25** with either of its prochiral planes exogonically yielding corresponding catalyst–substrate complexes **26** and **27** (Scheme 5). Endogonic coordination of molecular hydrogen giving complexes **28** and **29** is followed by oxidative addition to either the  $\alpha$ - or  $\beta$ -carbon atom of the double bond via transition states **TS14**–**TS17**.

In the case of an *si*-coordinated olefin, we failed to locate intermediate dihydrides, since the migratory insertion proceeded spontaneously, resulting in corresponding monohydrides **30** and **31**, which provided *R*-product coordinated to the catalyst via the corresponding transition states **TS18** and **TS19**. The corresponding dihydrides **32** and **33**, originating from the *re*-coordination of the double bond, were located together with the transition states for migratory insertion **TS20** and **TS21**. Nevertheless, the relative free energies of **TS20** and **TS21** are notably lower than those of **TS16** and **TS17**, and the presence of the additional step in the *S*-catalytic cycles does not affect the process of enantioselection (*vide infra*).

Inspection of Figure 4 makes it possible to conclude that the chirality is generated in the migratory insertion step via the difference in the free energies of **TS14**(*R*) and **TS17**(*S*) (Figure 5). Although in this case the reductive elimination becomes the rate-limiting stage, it does not affect the stereochemical outcome, since the difference in the free energies of the corresponding transition states (**TS18**(*R*) and either **TS22**(*S*) or **TS23**(*S*)) remains almost the same and for exactly the same reasons.

It is not easy to make a clear statement on which of the computed mechanisms is actually operating. The catalytic cycles are quite similar energetically (Figures 2 and 4). Each of them comprises a final stage with activation barriers around 25 kcal/mol (reductive elimination in the case of the Co(I)-Co(III) mechanism and H<sub>2</sub> metathesis in the case of Co(0)-Co(II) mechanism). Most probably, these two mechanisms can operate simultane-

ously in a manner that, in accord with the computational results, does not affect the almost perfect enantioselectivity observed in this reaction.



**Scheme 5.** Four competing pathways of Co(0)-Co(II) catalytic cycles proceeding via hydrogenation of catalyst-substrate complexes.

In either the Co(I)-Co(III) or the Co(0)-Co(II) mechanism, the *R*-enantioselectivity is secured via C-H $\cdots\pi$  interactions between the triple bond of the substrate and the *t*-Bu group of the catalyst. This means that the handedness of the asymmetric hydrogenation can be predicted without the need for detailed studies on the catalytic cycle, with the only reasonable assumption of the hydride coming from the side of the metal.



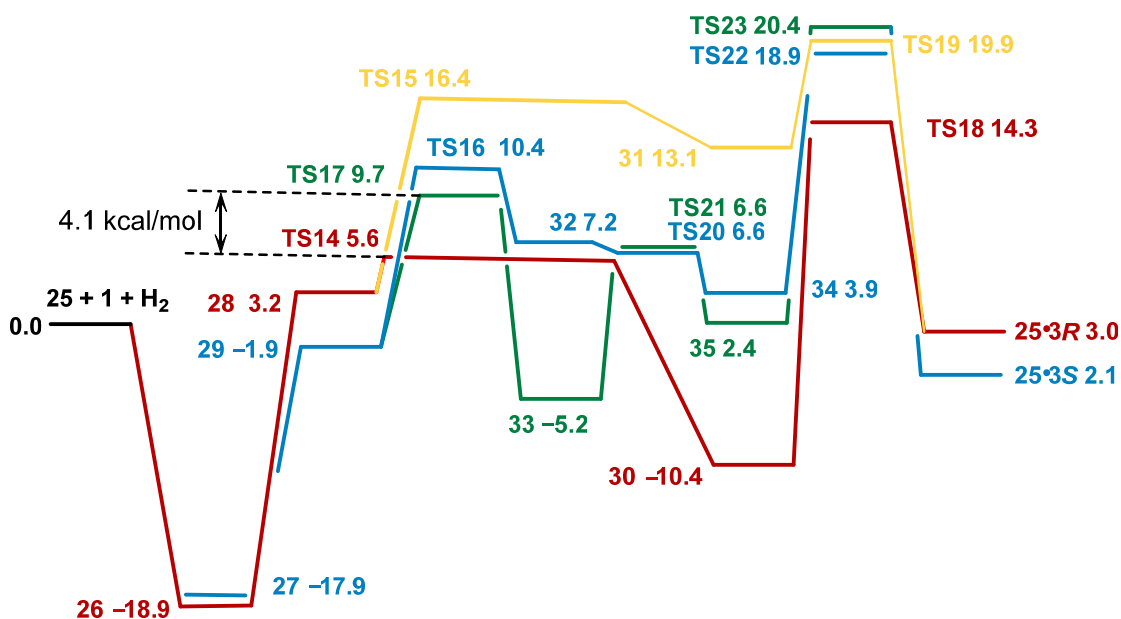


**Figure 4.** Profile of relative free energies (kcal/mol) in four competing catalytic cycles of the Ni(0)-Ni(II) route. Red—R(α), blue—S(α), yellow—R(β), green—S(β)

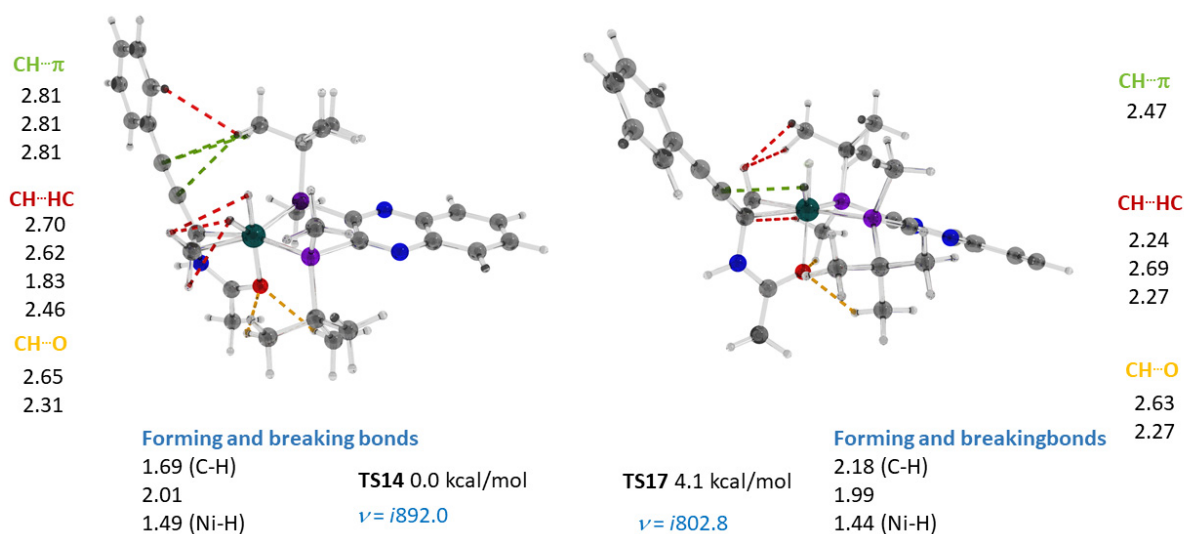


**Figure 5.** Optimized structures and important interatomic distances of the transition states TS4 and TS7. Black—C, grey—H, blue—N, red—O, violet—P, turquoise—Co.

Using the well-known quadrant diagrams introduced by Knowles [55], but bearing in mind that the *t*-Bu group, which is rich in C-H bonds, actually provides a stabilizing effect, although not repulsion, as previously thought [56], one can predict the handedness of the product by positioning a substrate with groups capable of rendering disperse interactions against the “bulky quadrants” of the catalyst and determining the sign of chirality in a typical way, suggesting that the hydrogen atom will come from the side of the metal.

This approach is exemplified in Figure 6. *R,R*-QuinoxP\* has *t*-Bu groups in the upper left and lower right quadrants. The *R*-configuration of the hydrogenation product can be predicted without detailed mechanistic studies, considering only the coordination of the substrate in an *octahedral complex*, upon which the groups capable for building disperse interactions with *t*-Bu substituents would be positioned in the same quadrants (Figure 6, left). In the same fashion, the *S*-configuration of the MACH<sub>2</sub> [35] can be predicted on the basis of the asymmetric hydrogenation with the *R,R*<sup>*i*-Pr</sup>DuPHOS-Rh complex.



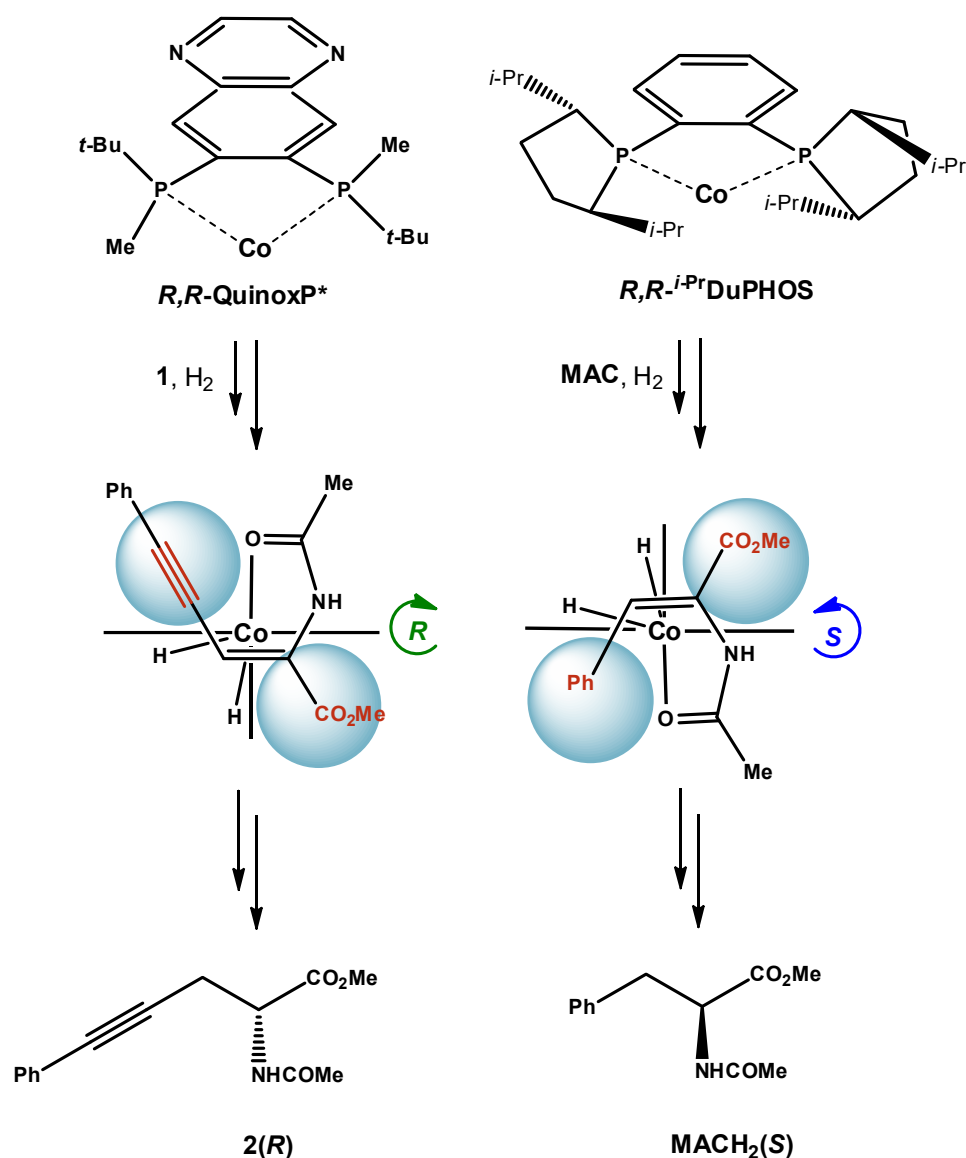


**Figure 6.** General scheme for predicting the handedness of asymmetric hydrogenation.

The same predictions are valid for numerous Rh-catalyzed asymmetric hydrogenations [7,8,11,12,33], with the notable exception of enamides with *t*-Bu or adamantyl substituent [57,58] that choose a  $\beta$ -coordination pathway [11,12,56,59].

### 3. Conclusions

The results reported in this paper suggest that the focus of the studies of the mechanisms of asymmetric catalytic hydrogenations could be somewhat different from the commonly accepted one. The catalytic activity important for breaking chemical bonds and forming new ones is certainly quite sensitive to the electronic states of transition metal atoms. On the other hand, the sense and level of enantioselection seem to be much less susceptible to redox processes. These considerations can provide an efficient and short way of arriving at important conclusions when only stereochemical information is required.

The author plans to study the further implications of the regularities reported in this paper.

## 4. Materials and Methods

### Computational Details

Geometry optimizations were performed without any symmetry constraints (C1 symmetry) using the  $\omega$ B97XD functional [60] as implemented in the Gaussian09 software package [61]. Frequency calculations were undertaken to confirm the nature of the stationary points, yielding one imaginary frequency for all transition states (TS) and zero for all minima. Constrained energy hypersurface scans were conducted to investigate the molecular reactivity and to locate viable reaction channels. Where low-lying barriers were estimated, frequency calculations were performed at the crude saddle points, and the obtained force constants were used to optimize the transition state structures by employing the Berny algorithm [62]. All atoms were described using the 6-31G\*\* basis set for geometry optimization and frequency calculation [63–68]. In the calculation of single-point energies, all atoms were described using the 6-311++G\*\* basis set [69–73]. Non-specific solvation was introduced using the SMD continuum model [74] (acetonitrile). Cartesian coordinates of all optimized intermediates and transition states are given in the Supporting Information.

**Supplementary Materials:** The following supporting information can be downloaded at: <https://www.mdpi.com/article/10.3390/ijms24065568/s1>.

**Funding:** This research received no external funding.

**Institutional Review Board Statement:** Not applicable.

**Informed Consent Statement:** Not applicable.

**Data Availability Statement:** Not applicable.

**Conflicts of Interest:** The author declares no conflict of interest.

## References

1. Hartwig, J. *Organotransition Metal Chemistry: From Bonding to Catalysis*, 1st ed.; University Science Books: Sausalito, CA, USA, 2009.
2. Barton, A. *Organometallic Transition Metal Catalysis: A Hostic Approach to Understanding and Predicting Their Mechanisms*; Lulu: Kerala, India, 2022.
3. Brown, J.M. *Hydrogenation of Functionalized Carbon-Carbon Double Bonds*; Jacobsen, E.N., Pfaltz, A., Yamamoto, H., Eds.; Springer: Berlin/Heidelberg, Germany, 1999; Volume 1, pp. 119–182.
4. Halpern, J. Mechanism of Stereoselectivity of Asymmetric Hydrogenation. *Science* **1982**, *217*, 401–407. [[CrossRef](#)] [[PubMed](#)]
5. Landis, C.R.; Halpern, J. Asymmetric Hydrogenation of Methyl-(Z)- $\alpha$ -acetamidocinnamate Catalyzed by {1,2-Bis((phenyl-*o*-anisoyl)phosphino)ethane}rhodium(I): Kinetics, Mechanism, and Origin of Enantioselection. *J. Am. Chem. Soc.* **1987**, *109*, 1746–1754. [[CrossRef](#)]
6. Giernoth, R.; Heinrich, H.; Adams, N.J.; Deeth, R.J.; Bargon, J.; Brown, J.M. Phip Detection of a Transient Rhodium Dihydride Intermediate in the Homogeneous Hydrogenation of Dehydroamino Acids. *J. Am. Chem. Soc.* **2000**, *122*, 12381–12382. [[CrossRef](#)]
7. Gridnev, I.D.; Imamoto, T. On the Mechanism of Stereoselection in Rh-Catalyzed Asymmetric Hydrogenation: A General Approach for Predicting the Sense of Enantioselectivity. *Acc. Chem. Res.* **2004**, *37*, 633–644. [[CrossRef](#)] [[PubMed](#)]
8. Gridnev, I.D.; Imamoto, T. Mechanism of Enantioselection in Rh-Catalyzed Asymmetric Hydrogenation. The Origin of Utmost Catalytic Performance. *Chem. Commun.* **2009**, 7447–7464. [[CrossRef](#)]
9. Verdolino, V.; Forbes, A.; Helquist, P.; Norrby, P.-O.; Wiest, O. On the mechanism of the rhodium catalyzed acrylamide hydrogenation. *J. Mol. Catal. A Chem.* **2010**, *324*, 9–14. [[CrossRef](#)]
10. Imamoto, T.; Tamura, K.; Zhang, Z.; Horiuchi, Y.; Sugiya, M.; Yoshida, K.; Yanagisawa, A.; Gridnev, I.D. Rigid P-chiral phosphine ligands with *tert*-butylmethylphosphino groups for rhodium-catalyzed asymmetric hydrogenation of functionalized alkenes. *J. Am. Chem. Soc.* **2012**, *134*, 1754–1769. [[CrossRef](#)]
11. Gridnev, I.D.; Imamoto, T. Challenging the major/minor concept in Rh-catalyzed asymmetric hydrogenation. *ACS Catal.* **2015**, *5*, 2911–2915. [[CrossRef](#)]
12. Gridnev, I.D.; Dub, P.A. *Enantioselection in Asymmetric Catalysis*; CRC Press: Boca Raton, FL, USA, 2016; p. 234.
13. Kitamura, M.; Tsukamoto, M.; Bessho, Y.; Yoshimura, M.; Kobs, U.; Widhalm, M.; Noyori, R. Mechanism of Asymmetric Hydrogenation of  $\alpha$ -(Acylamino)acrylic Esters Catalyzed by BINAP-Ruthenium(II) Diacetate. *J. Am. Chem. Soc.* **2002**, *124*, 6649–6667. [[CrossRef](#)]
14. Dub, P.A.; Gordon, J.C. The role of the metal-bound N–H functionality in Noyori-type molecular catalysts. *Nat. Rev. Chem.* **2018**, *2*, 396–408. [[CrossRef](#)]

15. Dub, P.A.; Ikariya, T. Quantum Chemical Calculations with the Inclusion of Nonspecific and Specific Solvation: Asymmetric Transfer Hydrogenation with Bifunctional Ruthenium Catalysts. *J. Am. Chem. Soc.* **2013**, *135*, 2604–2619. [\[CrossRef\]](#) [\[PubMed\]](#)
16. Dub, P.A.; Gordon, J.C. The mechanism of enantioselective ketone reduction with Noyori and Noyori–Ikariya bifunctional catalysts. *Dalton Trans* **2016**, *45*, 6756–6781. [\[CrossRef\]](#)
17. Roseblade, J.; Pfaltz, A. Iridium-catalyzed asymmetric hydrogenation of olefins. *Acc. Chem. Res.* **2007**, *40*, 1402–1411. [\[CrossRef\]](#) [\[PubMed\]](#)
18. Hopmann, K.H.; Bayer, A. On the Mechanism of Iridium-Catalyzed Asymmetric Hydrogenation of Imines and Alkenes: A Theoretical Study. *Organometallics* **2011**, *30*, 2483–2497. [\[CrossRef\]](#)
19. Liu, Y.; Gridnev, I.D.; Zhang, W. Mechanism of Asymmetric Hydrogenation of Exocyclic  $\alpha$ ,  $\beta$ -Unsaturated Carbonyl Compounds with an Iridium/Biphosphox Catalyst: NMR and DFT Studies. *Angew. Chem. Intl. Ed.* **2014**, *53*, 1901–1905. [\[CrossRef\]](#)
20. Sparta, M.; Riplinger, C.; Neese, F. Mechanism of Olefin Asymmetric Hydrogenation Catalyzed by Iridium Phosphino-Oxazoline: A Pair Natural Orbital Coupled Cluster Study. *J. Chem. Theory Comput.* **2014**, *10*, 1099–1108. [\[CrossRef\]](#) [\[PubMed\]](#)
21. Tutkowski, B.; Kerdphon, S.; Limé, E.; Helquist, P.; Andersson, P.G.; Wiest, O.; Norrby, P.-O. Revisiting the Stereodetermining Step in Enantioselective Iridium-Catalyzed Imine Hydrogenation. *ACS Catal.* **2018**, *8*, 615–623. [\[CrossRef\]](#)
22. Cui, C.X.; Chen, H.H.; Li, S.J.; Zhang, T.; Qu, L.B.; Lan, Y. Mechanism of Ir-catalyzed hydrogenation: A theoretical view. *Coord. Chem. Rev.* **2020**, *412*, 213251. [\[CrossRef\]](#)
23. Mas-Roselló, J.; Smejkal, T.; Cramer, N. Iridium-catalyzed acid-assisted asymmetric hydrogenation of oximes to hydroxylamines. *Science* **2020**, *368*, 1098–1102. [\[CrossRef\]](#)
24. Vogiatzis, K.D.; Polynski, M.V.; Kirkland, J.K.; Townsend, J.; Hashemi, A.; Liu, C.; Pidko, E.A. Computational Approach to Molecular Catalysis by 3d Transition Metals: Challenges and Opportunities. *Chem. Rev.* **2019**, *119*, 2453–2523. [\[CrossRef\]](#)
25. Zhang, Z.; Butt, N.A.; Zhou, M.; Liu, D.; Zhang, W. Asymmetric Transfer and Pressure Hydrogenation with Earth-Abundant Transition Metal Catalysts. *Chin. J. Chem.* **2018**, *36*, 443–454. [\[CrossRef\]](#)
26. Seo, C.S.G.; Morris, R.H. Catalytic Homogeneous Asymmetric Hydrogenation: Successes and Opportunities. *Organometallics* **2019**, *38*, 47–65. [\[CrossRef\]](#)
27. Li, B.; Chen, J.; Zhang, Z.; Gridnev, I.D.; Zhang, W. Nickel-catalyzed asymmetric hydrogenation of *N*-sulfonyl imines. *Angew. Chem. Intl. Ed.* **2019**, *58*, 7329–7334. [\[CrossRef\]](#)
28. Liu, Y.; Dong, X.-Q.; Zhang, X. Recent advances of nickel-catalyzed homogeneous asymmetric hydrogenation. *Chin. J. Org. Chem.* **2020**, *40*, 1096–1104. [\[CrossRef\]](#)
29. Hu, Y.; Chen, J.; Li, B.; Zhang, Z.; Gridnev, I.D.; Zhang, W. Nickel-catalyzed asymmetric hydrogenation of 2-amidoacrylates. *Angew. Chem. Intl. Ed.* **2020**, *59*, 5371–5375. [\[CrossRef\]](#) [\[PubMed\]](#)
30. Liu, D.; Li, B.; Chen, J.; Gridnev, I.D.; Yan, D.; Zhang, W. Ni-catalyzed asymmetric hydrogenation of *N*-aryl imino esters for the efficient synthesis of chiral  $\alpha$ -aryl glycines. *Nat. Commun.* **2020**, *11*, 5935. [\[CrossRef\]](#)
31. Li, B.; Chen, J.; Liu, D.; Gridnev, I.D.; Zhang, W. Nickel-catalysed asymmetric hydrogenation of oximes. *Nat. Chem.* **2022**, *14*, 920–927. [\[CrossRef\]](#)
32. Monfette, S.; Turner, Z.R.; Semproni, S.P.; Chirik, P.J. Enantiopure C1-Symmetric Bis(imino)pyridine Cobalt Complexes for Asymmetric Alkene Hydrogenation. *J. Am. Chem. Soc.* **2012**, *134*, 4561–4564. [\[CrossRef\]](#)
33. Zhang, G.; Vasudevan, K.V.; Scott, B.L.; Hanson, S.K. Understanding the Mechanisms of Cobalt-Catalyzed Hydrogenation and Dehydrogenation Reactions. *J. Am. Chem. Soc.* **2013**, *135*, 8668–8681. [\[CrossRef\]](#)
34. Zhong, H.; Friedfeld, M.R.; Chirik, P.J. Syntheses and Catalytic Hydrogenation Performance of Cationic Bis(phosphine) Cobalt(I) Diene and Arene Compounds. *Angew. Chem. Intl. Ed.* **2019**, *58*, 9194–9198. [\[CrossRef\]](#) [\[PubMed\]](#)
35. Hopmann, K.H. Cobalt–Bis(imino)pyridine-Catalyzed Asymmetric Hydrogenation: Electronic Structure, Mechanism, and Stereoselectivity. *Organometallics* **2013**, *32*, 6388–6399. [\[CrossRef\]](#)
36. Zhong, H.; Friedfeld, M.R.; Camacho-Bunquin, J.; Sohn, H.; Yang, C.; Delferro, M.; Chirik, P.J. Exploring the Alcohol Stability of Bis(phosphine) Cobalt Dialkyl Precatalysts in Asymmetric Alkene Hydrogenation. *Organometallics* **2019**, *38*, 149–156. [\[CrossRef\]](#)
37. Friedfeld, M.R.; Zhong, H.; Ruck, R.T.; Shevlin, M.; Chirik, P.J. Cobalt-catalyzed asymmetric hydrogenation of enamides enabled by single-electron reduction. *Science* **2018**, *360*, 888–893. [\[CrossRef\]](#)
38. Chen, J.; Chen, C.; Ji, C.; Lu, Z. Cobalt-Catalyzed Asymmetric Hydrogenation of 1,1-Diarylethenes. *Org. Lett.* **2016**, *18*, 1594–1597. [\[CrossRef\]](#) [\[PubMed\]](#)
39. Friedfeld, M.R.; Shevlin, M.; Margulieux, G.W.; Campeau, L.-C.; Chirik, P.J. Cobalt-Catalyzed Enantioselective Hydrogenation of Minimally Functionalized Alkenes: Isotopic Labeling Provides Insight into the Origin of Stereoselectivity and Alkene Insertion Preferences. *J. Am. Chem. Soc.* **2016**, *138*, 3314–3324. [\[CrossRef\]](#) [\[PubMed\]](#)
40. Ma, X.; Lei, M. Mechanistic Insights into the Directed Hydrogenation of Hydroxylated Alkene Catalyzed by Bis(phosphine)Cobalt Dialkyl Complexes. *J. Org. Chem.* **2017**, *82*, 2703–2712. [\[CrossRef\]](#)
41. Hu, Y.; Zhang, Z.; Zhang, J.; Liu, Y.; Gridnev, I.D.; Zhang, W. Cobalt-Catalyzed Asymmetric Hydrogenation of C=N Bonds Enabled by Assisted Coordination and Nonbonding Interactions. *Angew. Chem. Intl. Ed.* **2019**, *58*, 15767–15771. [\[CrossRef\]](#)
42. Zhong, H.; Shevlin, M.; Chirik, P.J. Cobalt-Catalyzed Asymmetric Hydrogenation of  $\alpha,\beta$ -Unsaturated Carboxylic Acids by Homolytic H<sub>2</sub> Cleavage. *J. Am. Chem. Soc.* **2020**, *142*, 5272–5281. [\[CrossRef\]](#) [\[PubMed\]](#)

43. Du, X.; Xiao, Y.; Yang, Y.; Duan, Y.-N.; Li, F.; Hu, Q.; Chung, L.W.; Chen, G.-Q.; Zhang, X. Enantioselective Hydrogenation of Tetrasubstituted  $\alpha,\beta$ -Unsaturated Carboxylic Acids Enabled by Cobalt(II) Catalysis: Scope and Mechanistic Insights. *Angew. Chem. Int. Ed.* **2021**, *60*, 11384–11390. [[CrossRef](#)]
44. Du, X.; Xiao, Y.; Huang, J.-M.; Zhang, Y.; Duan, Y.-N.; Wang, H.; Shi, C.; Chen, G.-Q.; Zhang, X. Cobalt-catalyzed highly enantioselective hydrogenation of  $\alpha,\beta$ -unsaturated carboxylic acids. *Nat. Commun.* **2020**, *11*, 3239. [[CrossRef](#)] [[PubMed](#)]
45. Hu, Y.; Zhang, Z.; Liu, Y.; Zhang, W. Cobalt-Catalyzed Chemo- and Enantioselective Hydrogenation of Conjugated Enynes. *Angew. Chem. Int. Ed.* **2021**, *60*, 16989–16993. [[CrossRef](#)] [[PubMed](#)]
46. Mendelsohn, L.N.; Pavlovic, L.; Zhong, H.; Friedfeld, M.R.; Shevlin, M.; Hopmann, K.H.; Chirik, P.J. Mechanistic Investigations of the Asymmetric Hydrogenation of Enamides with Neutral Bis(phosphine) Cobalt Precatalysts. *J. Am. Chem. Soc.* **2022**, *144*, 15764–15778. [[CrossRef](#)]
47. Pavlovich, L.; Mendelsohn, L.N.; Zhong, H.Y.; Chirik, P.J.; Hopmann, K.H. Cobalt-Catalyzed Asymmetric Hydrogenation of Enamides: Insights into Mechanisms and Solvent Effects. *Organometallics* **2022**, *41*, 1872–1882. [[CrossRef](#)]
48. Zhou, S.; Fleischer, S.; Junge, K.; Das, S.; Addis, D.; Beller, M. Enantioselective Synthesis of Amines: General, Efficient Iron-Catalyzed Asymmetric Transfer Hydrogenation of Imines. *Angew. Chem. Int. Ed.* **2010**, *49*, 8121–8125. [[CrossRef](#)] [[PubMed](#)]
49. Lagaditis, P.O.; Sues, P.E.; Sonnenberg, J.F.; Wan, K.Y.; Lough, A.J.; Morris, R.H. Iron(II) Complexes Containing Unsymmetrical P–N–P' Pincer Ligands for the Catalytic Asymmetric Hydrogenation of Ketones and Imines. *J. Am. Chem. Soc.* **2014**, *136*, 1367–1380. [[CrossRef](#)]
50. Smith, S.A.M.; Lagaditis, P.O.; Lüpke, A.; Lough, A.J.; Morris, R.H. Unsymmetrical Iron P–NH–P' Catalysts for the Asymmetric Pressure Hydrogenation of Aryl Ketones. *Chem.-Eur. J.* **2017**, *23*, 7212–7216. [[CrossRef](#)]
51. Sonnenberg, J.F.; Wan, K.Y.; Sues, P.E.; Morris, R.H. Ketone Asymmetric Hydrogenation Catalyzed by P–NH–P' Pincer Iron Catalysts: An Experimental and Computational Study. *ACS Catal.* **2017**, *7*, 316–326. [[CrossRef](#)]
52. Seo, C.S.G.; Tannoux, T.; Smith, S.A.M.; Lough, A.J.; Morris, R.H. Enantioselective hydrogenation of activated aryl imines catalyzed by an iron(II) P–NH–P' complex. *J. Org. Chem.* **2019**, *84*, 12040–12049. [[CrossRef](#)]
53. Zhang, L.; Tang, Y.; Han, Z.; Ding, K. Lutidine-based chiral pincer manganese catalysts for enantioselective hydrogenation of ketones. *Angew. Chem. Int. Ed.* **2019**, *58*, 4973–4977. [[CrossRef](#)]
54. Zhang, L.; Wang, Z.; Han, Z.; Ding, K. Manganese-catalyzed anti-selective asymmetric hydrogenation of  $\alpha$ -substituted  $\beta$ -ketoamides. *Angew. Chem. Int. Ed.* **2020**, *59*, 15565–15569. [[CrossRef](#)]
55. Knowles, W.S. Asymmetric Hydrogenation. *Acc. Chem. Res.* **1983**, *16*, 106–112. [[CrossRef](#)]
56. Gridnev, I.D. Attraction versus Repulsion in Rhodium-Catalyzed Asymmetric Hydrogenation. *ChemCatChem* **2016**, *8*, 3463–3468. [[CrossRef](#)]
57. Burk, M.J.; Casy, G.; Johnson, N.B. A Three-Step Procedure for Asymmetric Catalytic Reductive Amidation of Ketones. *J. Org. Chem.* **1998**, *63*, 6084–6085. [[CrossRef](#)]
58. Gridnev, I.D.; Higashi, N.; Imamoto, T. On the Origin of opposite Stereoselection in the Asymmetric Hydrogenation of Phenyl- and *tert*-Butyl-Substituted Enamides. *J. Am. Chem. Soc.* **2000**, *122*, 10486–10487. [[CrossRef](#)]
59. Gridnev, I.D.; Yasutake, M.; Higashi, N.; Imamoto, T. Asymmetric Hydrogenation of Enamides with Rh-BisP\* and Rh-MiniPHOS Catalysts. Scope, Limitations, and Mechanism. *J. Am. Chem. Soc.* **2001**, *123*, 5268–5276. [[CrossRef](#)]
60. Chai, J.-D.; Head-Gordon, M. Long-Range Corrected Hybrid Density Functionals with Damped Atom–Atom Dispersion Corrections. *Phys. Chem. Chem. Phys.* **2008**, *10*, 6615–6620. [[CrossRef](#)]
61. Frisch, M.J.; Trucks, G.W.; Schlegel, H.B.; Scuseria, G.E.; Robb, M.A.; Cheeseman, J.R.; Scalmani, G.; Barone, V.; Mennucci, B.; Petersson, G.A.; et al. *Gaussian 09, rev. D.01*; Gaussian, Inc.: Wallingford, CT, USA, 2013.
62. Becke, A.D. Density-functional exchange-energy approximation with correct asymptotic behavior. *Phys. Rev. A* **1988**, *38*, 3098–3100. [[CrossRef](#)]
63. Ditchfield, R.; Hehre, W.J.; Pople, J.A. Self-Consistent Molecular-Orbital Methods. IX. An Extended Gaussian-Type Basis for Molecular-Orbital Studies of Organic Molecules. *J. Chem. Phys.* **1971**, *54*, 724–728. [[CrossRef](#)]
64. Hehre, W.J.; Ditchfield, R.; Pople, J.A. Self-Consistent Molecular Orbital Methods. XII. Further Extensions of Gaussian-Type Basis Sets for Use in Molecular Orbital Studies of Organic Molecules. *J. Chem. Phys.* **1972**, *56*, 2257–2261. [[CrossRef](#)]
65. Hariharan, P.C.; Pople, J.A. The influence of polarization functions on molecular orbital hydrogenation energies. *Theor. Chim. Acta* **1973**, *28*, 213–222. [[CrossRef](#)]
66. Francl, M.M.; Pietro, W.J.; Hehre, W.J.; Binkley, J.S.; Gordon, M.S.; DeFrees, D.J.; Pople, J.A. Self-consistent molecular orbital methods. XXIII. A polarization-type basis set for second-row elements. *J. Chem. Phys.* **1982**, *77*, 3654–3665.
67. Gordon, M.S.; Binkley, J.S.; Pople, J.A.; Pietro, W.J.; Hehre, W.J. Self-consistent molecular-orbital methods. 22. Small split-valence basis sets for second-row elements. *J. Am. Chem. Soc.* **1982**, *104*, 2797–2803. [[CrossRef](#)]
68. Rassolov, V.A.; Pople, J.A.; Ratner, M.A.; Windus, T.L. 6-31G\* basis set for atoms K through Zn. *J. Chem. Phys.* **1998**, *109*, 1223–1229. [[CrossRef](#)]
69. Krishnan, R.; Binkley, J.S.; Seeger, R.; Pople, J.A. Self-consistent molecular orbital methods. XX. A basis set for correlated wave functions. *J. Chem. Phys.* **1980**, *72*, 650–654. [[CrossRef](#)]
70. McLean, A.D.; Chandler, G.S. Contracted Gaussian basis sets for molecular calculations. I. Second row atoms, Z=11–18. *J. Chem. Phys.* **1980**, *72*, 5639–5648. [[CrossRef](#)]

71. Clark, T.; Chandrasekhar, J.; Spitznagel, G.W.; Schleyer, P.V.R. Efficient diffuse function-augmented basis sets for anion calculations. III. The 3-21+G basis set for first-row elements, Li–F. *J. Comput. Chem.* **1983**, *4*, 294–301. [[CrossRef](#)]
72. Spitznagel, G.W.; Clark, T.; Schleyer, P.V.R.; Hehre, W.J. An evaluation of the performance of diffuse function-augmented basis sets for second row elements, Na–Cl. *J. Comput. Chem.* **1987**, *8*, 1109–1116. [[CrossRef](#)]
73. Raghavachari, K.; Trucks, G.W. Highly correlated systems. Excitation energies of first row transition metals Sc–Cu. *J. Chem. Phys.* **1989**, *91*, 1062–1065. [[CrossRef](#)]
74. Marenich, A.V.; Cramer, C.J.; Truhlar, D.G. Universal Solvation Model Based on Solute Electron Density and on a Continuum Model of the Solvent Defined by the Bulk Dielectric Constant and Atomic Surface Tensions. *J. Phys. Chem. B* **2009**, *113*, 6378–6396. [[CrossRef](#)]

**Disclaimer/Publisher’s Note:** The statements, opinions and data contained in all publications are solely those of the individual author(s) and contributor(s) and not of MDPI and/or the editor(s). MDPI and/or the editor(s) disclaim responsibility for any injury to people or property resulting from any ideas, methods, instructions or products referred to in the content.